An annealing study of charge collection efficiency on Float-Zone p-on-n ministrip sensors irradiated with 24 GeV/c protons and 20 MeV neutrons

2015 JINST 10 P08005

(http://iopscience.iop.org/1748-0221/10/08/P08005)

PUBLISHED BY IOP PUBLISHING FOR SISSA MEDIALAB

RECEIVED: *March 3, 2015*
REVISED: *May 3, 2015*
ACCEPTED: *July 5, 2015*
PUBLISHED: *August 10, 2015*

An annealing study of charge collection efficiency on Float-Zone p-on-n ministrip sensors irradiated with 24 GeV/c protons and 20 MeV neutrons

N. Pacifico,[a,1,2] **I. Dolenc-Kittelmann,**[a,3] **M. Gabrysch,**[a,4] **C. Lucas**[b] **and M. Moll**[a]

[a] *CERN – European Center for Nuclear Research, 1211 Geneva 23, Switzerland*
[b] *University of Bristol, Bristol, U.K.*

E-mail: nicola.pacifico@cern.ch

ABSTRACT: Float-Zone n-bulk p-readout silicon sensors are currently operated in the tracking layers of many High Energy Physics experiments, where they are exposed to moderate to high fluences of hadrons. Though n-readout sensors, either with p or n bulk, are available and are offering an improved radiation hardness, p-on-n sensors are still widely used and are e.g. installed in the present ATLAS and CMS experiments at CERN. Their radiation hardness and long-term performance are therefore of high interest to the detector community.

We present here a study performed on these sensors after irradiation with 24 GeV/c protons and 20 MeV neutrons to fluences ranging from $1{\cdot}10^{14}$ to $1{\cdot}10^{15}$ n_{eq}/cm^2. The sensors were then investigated for charge collection efficiency after different isothermal annealing steps in order to understand the performance evolution of the sensor with annealing time. Additional measurements were performed for the highest neutron fluence by means of the Edge-TCT technique, to assess the electric field configuration within the sensor. The irradiation and the annealing scenarios were chosen to represent the radiation damage scenario over the expected lifetime of the LHC detectors (and even further) and to assess the effect of unplanned annealing due to potentially longer *warm* shutdowns or cooling problems.

KEYWORDS: Solid state detectors; Si microstrip and pad detectors; Radiation-hard detectors

[1] Corresponding author.
[2] Currently with University of Bergen, Allegt. 55, 5020 Bergen, Norway.
[3] Currently with European Spallation Source, Box 176 221 00 Lund, Sweden.
[4] Currently with University of Uppsala, Box 534 751 21 Uppsala, Sweden.

doi:10.1088/1748-0221/10/08/P08005

Contents

1 Introduction 1

2 Studied structures and irradiation experiments 2

3 CCE experimental set-up 5

4 CCE measurements and annealing study 6

5 Edge-TCT measurement 13

6 Discussion of results 15

2015 JINST 10 P08005

1 Introduction

After being introduced in the late 70's, silicon sensors have become the standard choice for the construction of inner tracking systems of High Energy Physics (HEP) experiments. Their superior performance in terms of timing and spatial resolution make them suitable for finding primary and secondary vertices through accurate tracking of charged particles. For finding secondary vertices silicon detectors are often located as close as a few cm or less from the interaction point. This however exposes those detectors to extremely high hadron fluences that, in the biggest two LHC experiments, ATLAS and CMS, are expected to reach up to about $2{\cdot}10^{15}\,n_{eq}/cm^2$ in the silicon pixel detectors [1, 2] and $2{\cdot}10^{14}\,n_{eq}/cm^2$ in the silicon strip trackers [2, 3]. Therefore, throughout the operation of the detectors, a loss in performance has to be anticipated. Several radiation damage effects impact on the silicon sensor performance:

- Increase in leakage current
- Increase in full depletion voltage (V_{dep})
- Increase of trapping probability for drifting charge carriers.

Apart from the first effect, which has obvious consequences on the increase of the power dissipated by the sensors and the increase of thermal (shot) noise, the last two effects have a direct impact on the signal formation. An increase in V_{dep} leads to the inability to fully deplete the sensor's bulk, thus reducing its active volume. Moreover, after irradiation, carriers are trapped in defects and are therefore not contributing anymore to the induced signal. For n-bulk, p-readout Float-Zone (FZ) silicon, the situation is further complicated by the radiation induced type inversion (space charge sign inversion) of the bulk [4], that causes the depleted region to develop from the side of the sensor which is opposite to the readout electrode. Since the region of the segmented sensors which mostly

contributes to the signal is the one closest to the readout electrodes (stronger weighting field) [5, 6], the loss of efficiency in the readout electrode region results in an important signal loss.

This last effect has led to the introduction of n-readout sensors on n-bulk for the regions exposed to the highest fluences (e.g. the inner pixel detectors of ATLAS and CMS). Here the n-bulk quickly type inverts to p-type with increasing irradiation (at fluences in the order of $10^{12} \div 10^{13}\,n_{eq}/cm^2$, depending from the initial bulk resitivity), thus shifting the region of high electric field from the backside to the segmented front electrode. The n-readout sensors also present the additional advantage of collecting electrons, leading to a lower trapping-induced charge loss, due to the higher mobility of electrons with respect to holes [7]. n-readout detectors with p-type bulk are also foreseen for the current upgrade programs of the Phase-II strip tracker upgrades of the LHC experiments, in order to cope with the significant increase in luminosity of the experiments [8, 9].

Nevertheless, radiation hardness of p-on-n sensors is still of high interest, as they are widely used in several trackers for High Energy Physics experiments and the ATLAS and CMS experiments are still accumulating radiation fluence leading to further performance degradation of the devices. A good understanding of their performance evolution with radiation is therefore relevant to their operation over the projected lifetime.

The radiation induced defects in the silicon crystal structure that cause these degradation effects are most often not stable and consequently lead to a change of the sensor properties with time. The mobility of defects in silicon or their transformation is usually accelerated exponentially with temperature, a process known as *annealing* [10]. Two stages are generally identified in the annealing process. In the first stage, known as *beneficial annealing*, part of the negative space charge generated by the defects is neutralized. Following this stage, the *reverse annealing* takes place, during which additional negative space charge is created in the sensor bulk [10]. Extensive data concerning the development of V_{dep} in FZ p-on-n sensors with irradiation and annealing can be found in literature. The most accepted parametrization, the so called *Hamburg Model*, can be found in [10]. Other phenomenological studies and parameterizations on Float Zone p-on-n diodes and ministrip sensor properties with irradiation and annealing have been proposed [11–15]. The study presented in [11], in particular, gives a first evaluation of annealing effects on the charge collection efficiency of irradiated diodes. A decrease in the cluster charge is observed in type-inverted sensors after long annealing times. The technical design reports of HEP experiments always account for the effects of annealing, with a strict planning of room-temperature maintenance periods of the irradiated silicon tracking and vertex detectors. The aim of this work is to study the performance of irradiated FZ p-readout, n-bulk strip sensors in terms of signal and noise charge after irradiation and during annealing and to assess the operational limits and related performance losses in a harsh radiation environment like the ones present at the different LHC experiments.

2 Studied structures and irradiation experiments

The sensors studied here were standard FZ n-bulk, p-readout ministrip sensors, manufactured by Hamamatsu (HPK) [16]. The sensors were 320 μm thick, with an active area of $1 \times 8\,cm^2$. The strips were AC coupled, with 80 μm pitch and 20 μm strip width.

Secondary Ion Mass Spectroscopy (SIMS) and Spreading Resistance (SR) measurements were performed at ITME-Warsaw (PL) [17] on an unirradiated pad device originating from the same

2015 JINST 10 P08005

wafer batch as the strip sensors studied in this work. The SIMS measurements allowed determination of the oxygen and carbon concentration, which are known to have an impact on the silicon sensor radiation damage [18, 19]. It has been reported that a high carbon concentration leads to a faster increase of the depletion voltage with irradiation [18]. On the other hand, oxygen has been shown to have a beneficial effect in reducing the increase of depletion voltage with increasing charged hadron radiation levels, while in most neutron irradiation experiments no impact of the oxygen content has been found [19]. This effect and its dependence on the type of particle used for the irradiation experiment has been the subject of a recent study [20]. Radiation induced positively charged microscopic defects with enhanced production rate in oxygen rich material counterbalance the radiation induced negative space charge. These defects are point defects which are predominantly created after charged particle irradiation.

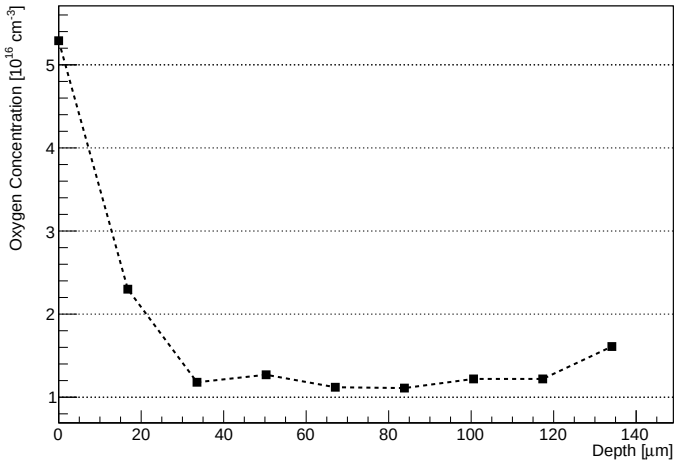

Figure 1. Oxygen concentration profile. The data were obtained by means of SIMS measurements.

The oxygen concentration as measured by the SIMS method is shown in figure 1. Technical constraints limited the depth scan to the first $\sim 135\,\mu$m starting from the front side. The oxygen concentration shows a gradient, with a higher concentration close to the electrode implant. There is evidence for oxygen diffusion from the silicon oxide surface layers during the high temperature steps of the sensor processing. Spreading resistance measurements were performed as well. The resulting resistivity and corresponding N_{eff} (effective doping concentration), vs. depth is shown in figure 2 for the first $\sim$200 μm on the front (junction) side. The spatial resolution of the measurement was not good enough to resolve the implant at the front junction and the first data point taken at the top surface ($450\,m\Omega \cdot$ cm) is omitted in the plot. The doping shows a good uniformity throughout the whole sensor bulk. The average resistivity is $1.71 \cdot 10^3\,\Omega$·cm, corresponding to an initial depletion voltage of ~ 210 V. The SIMS and SR measurements confirm that the sensor material can be regarded as reasonably typical high-resistivity Float Zone silicon.

The irradiation was performed at two different facilities: CERN PS irradiation facility (24 GeV/c protons) [21] and the Louvain-La-Neuve (BE) neutron facility (20 MeV neutrons) [22]. Proton and neutron fluences were chosen to have the same values when scaled to the 1 MeV neutron

2015 JINST 10 P08005

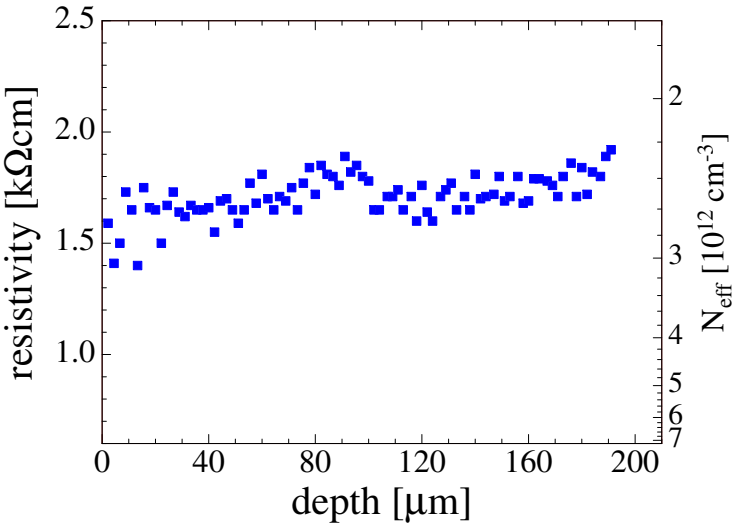

Figure 2. Resistivity as obtained with the spreading resistance method. The corresponding N_{eff} is given on the right hand y-axis. Experimental errors are smaller than markers on this scale.

equivalent fluence and are listed in table 1. While the sensors were cooled down to below $-20°C$ during neutron irradiations, the proton irradiations were performed at room temperature and lasted up to one week at $\sim 25°C$ for the sensor irradiated to the highest fluence. When evaluating the data it should be remembered that a part of the beneficial annealing has already taken place during irradiation with protons.

Table 1 also provides the depletion voltages of the detectors before irradiation with the exception of the sample with the lowest neutron fluence, for which the depletion voltage was not measured before irradiation.

Table 1. List of irradiated strip sensors. The last sensor was irradiated with a mixture of protons and neutrons (first $2{\cdot}10^{14}$ n_{eq}/cm^2 neutrons and then $3{\cdot}10^{14}$ n_{eq}/cm^2 protons).

$V_{dep,\phi=0}$ (V)	Fluence (n_{eq}/cm^2)	Particles	Error (%)
-	$1.0 \cdot 10^{14}$	neut.	7
142	$3.0 \cdot 10^{14}$	neut.	7
110	$5.0 \cdot 10^{14}$	neut.	14
110	$10.0 \cdot 10^{14}$	neut.	14
110	$1.0 \cdot 10^{14}$	prot.	7
215	$3.0 \cdot 10^{14}$	prot.	7
145	$5.0 \cdot 10^{14}$	prot.	7
175	$10 \cdot 10^{14}$	prot.	7
211	$5.0 \cdot 10^{14}$	mix.	20

Since in actual HEP experiments the particle flux is a mixture of different kind of particles, one sensor was exposed to a mixed irradiation with both protons and neutrons, up to a total fluence of $5{\cdot}10^{14}$ n_{eq}/cm^2 (first $2{\cdot}10^{14}$ n_{eq}/cm^2 neutrons and then $3{\cdot}10^{14}$ n_{eq}/cm^2 protons). All sensors were stored after irradiation at low temperature ($< 0°C$) to prevent unplanned annealing.

3 CCE experimental set-up

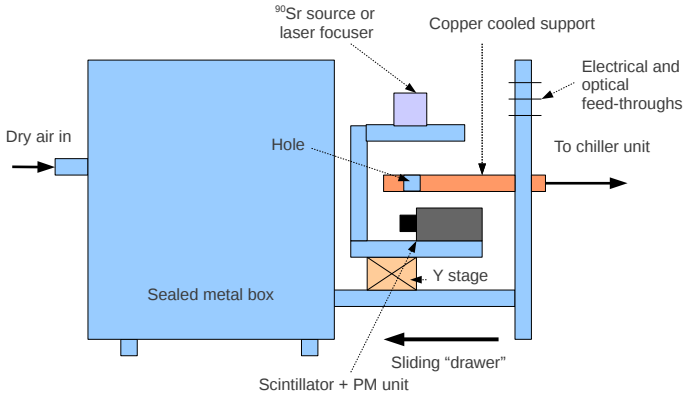

Figure 3. Schematic drawing of the set-up used for CCE measurements.

The Alibava [23] based set-up, used for the Charge Collection Efficiency (CCE) measurements presented here, is thoroughly described in [24]. A schematic representation of the set-up is provided in figure 3. The purpose of this set-up is the measurement of the charge generated in the sensor by impinging MIPs (minimum ionizing particles), in this case β particles generated by a radioactive source. The expected charge generated in a 320 μm silicon by a MIP is ∼25000 e-h pairs. The set-up makes use of a 3.6 MBq ^{90}Sr source, allowing a recorded event rate of ∼ 100 Hz, and implements a cooling system that, along with a dry air flushing, can allow measurements down to a temperature of $-30°C$ with a stability $\pm 1°C$. The temperature chosen for the measurements shown in the following section was $-20°C$, in order to keep the leakage current below the compliance limit of the bias supply (1 mA) even for the most irradiated sensors. Current measurements were taken throughout the acquisition to monitor the thermal stability of the sensor. However it was not possible to measure the bulk leakage current, as the high voltage was applied to the ohmic side of the sensor and the guard ring was left floating. The CCE analysis was performed with a customized version of the ROOT macros provided with the Alibava system [23]. The analysis of the cluster charge was performed by setting a threshold of $3{\cdot}ENC$ (Equivalent Noise Charge — ∼1200 e^-) for the seed strip. Neighboring channels were added to the cluster if their charge was exceeding $1.5{\cdot}ENC$. Annealing steps were performed by placing the sensor together with the mounting PCB and support into an oven at a controlled temperature of 60°C. The acceleration factors for the annealing of the effective doping concentration at this temperature, with respect to standard room temperature (20°C), are 174 for the short term component and 544 for the long term component corresponding to activation energies of respectively (1.09 ± 0.03) and 1.33 ± 0.03 eV, as found in [10].

2015 JINST 10 P08005

4 CCE measurements and annealing study

The most probable values (MPVs) of cluster charge were analysed and plotted as function of voltage for the different sensors at the different annealing stages. Figure 4 provides an example on how the MPVs of the cluster charge distribution curves were obtained by fitting a Landau convoluted with a Gaussian function to the curve.

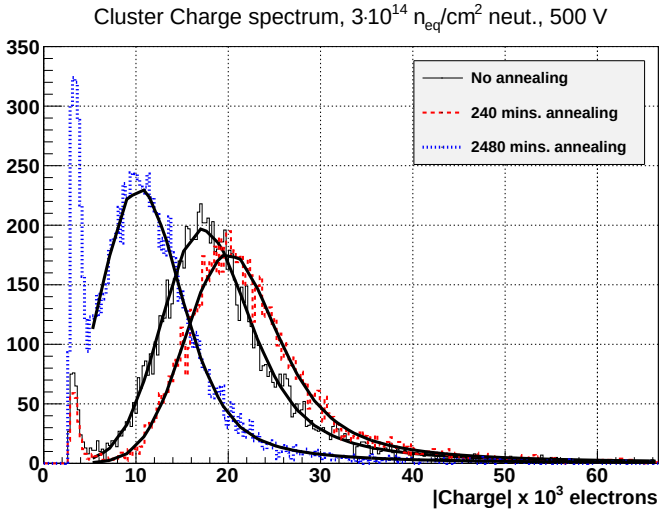

Figure 4. Cluster charge distribution at 500 V for the sensor irradiated to $3 \cdot 10^{14}$ n_{eq}/cm^2 neutrons, at three different annealing steps. Seed and neighbour cuts were reduced in this plot to $2 \cdot ENC$ and $1.5 \cdot ENC$ respectively to show the gaussian noise tail overalapping with the signal. The fits of the Landau function convoluted with a Gaussian function are shown as well.

Cluster charge MPVs versus bias voltage are shown in figures 5 to 11 for all the sensors with the exception of the two irradiated to the minimum and maximum proton fluences ($1 \cdot 10^{14}$ and $1 \cdot 10^{15}$ n_{eq}/cm^2). For these ones an early breakdown (starting at 100 V and 300 V, respectively) prevented charge collection efficiency studies.

The cluster charge plot for the $1 \cdot 10^{14} n_{eq}/cm^2$ neutron irradiated sensor is shown in figure 5. The value of the full depletion voltage immediately after irradiation is $\sim$ 190 V. After 5040 minutes of annealing, an increase of V_{dep} of $\sim$150 V is observed, indicating that the sensor already went through space charge sign inversion. However, even after such long annealing times, the signal at 500 V remains almost constant, with a maximum variation of 5% of the cluster charge over the whole annealing range.

The CCE curves for the sensor irradiated with neutrons to $3 \cdot 10^{14} n_{eq}/cm^2$ are shown in figure 6 for the different annealing times. The V_{dep} extracted from the curve immediately after irradiation is about 610 V. After the first two annealing steps (80 and 240 minutes) the full depletion voltage is reduced to $\sim$ 480 V. Further annealing brings the sensor in the reverse annealing region, with a depletion voltage that shifts above the highest applied voltage.

Figure 7 shows the CCE for the sensor irradiation with neutrons to $5 \cdot 10^{14} n_{eq}/cm^2$. The irradiation has moved the depletion voltage before annealing to $\sim$ 850 V, with a cluster charge of $\sim$ 9000 e at 500 V. Also in this case, beneficial annealing shifts the V_{dep} to a lower value ($\sim$ 620 V).

2015 JINST 10 P08005

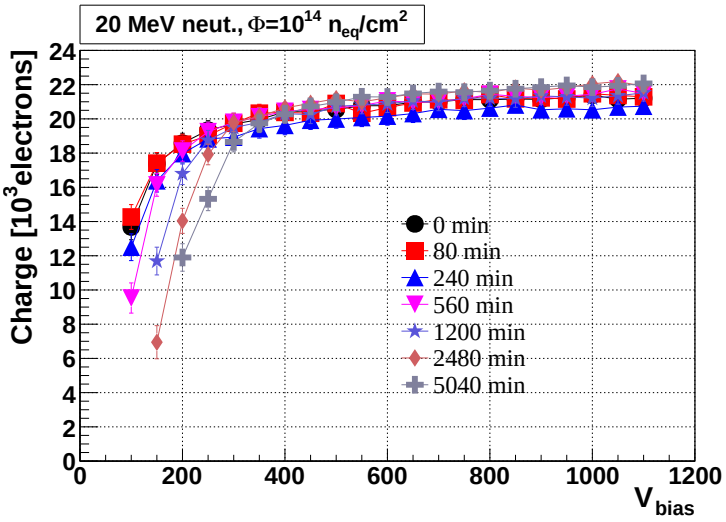

Figure 5. Cluster charge vs. V_{bias} at different annealing steps for the sensor irradiated with neutrons at $1{\cdot}10^{14}\,n_{eq}/cm^2$.

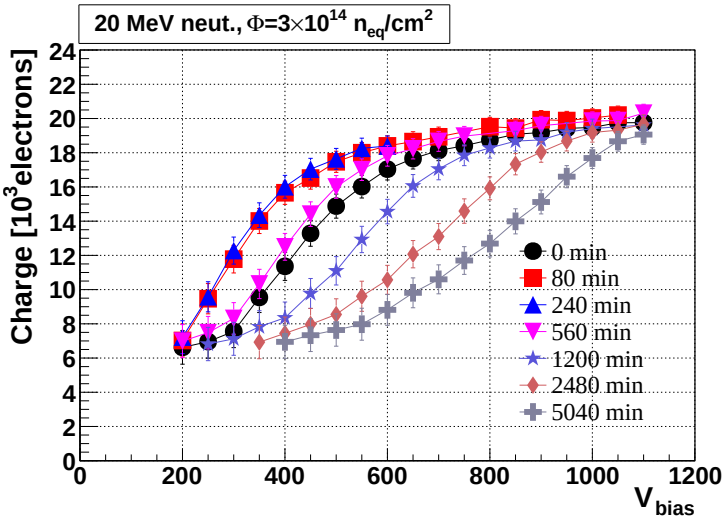

Figure 6. Cluster charge vs. V_{bias} at different annealing steps for the sensor irradiated with neutrons at $3{\cdot}10^{14}\,n_{eq}/cm^2$.

Further annealing brings the V_{dep} well above the bias supply limits, while the cluster charge at 500 V drops to $\sim$ 5500 e, which corresponds to a signal-to-noise ratio of less than 5 and did not allow to properly determine the most probable cluster charge value.

The data for the highest neutron fluence, far above the expected integrated fluence for strip detectors at the LHC, are shown in figure 8. At this fluence, the cluster charge at 500 V is $\sim$ 6000 e. Beneficial annealing shows a slight improvement in the cluster charge at this voltage, though with reverse annealing the signal becomes lower again.

The data for the proton irradiated sensors are shown in figures 9 and 10. When compared to corresponding neutron fluences (figures 6 and 7), both show a significantly lower depletion voltage

2015 JINST 10 P08005

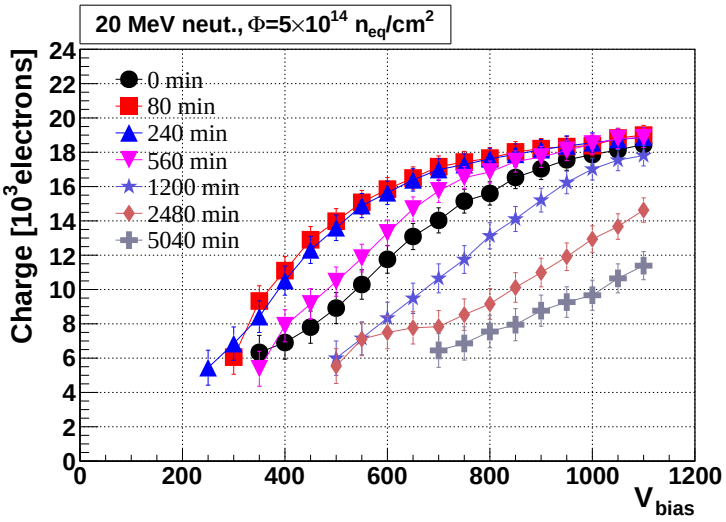

Figure 7. Cluster charge vs. V_{bias} at different annealing steps for the sensor irradiated with neutrons at $5{\cdot}10^{14}\,n_{eq}/cm^2$.

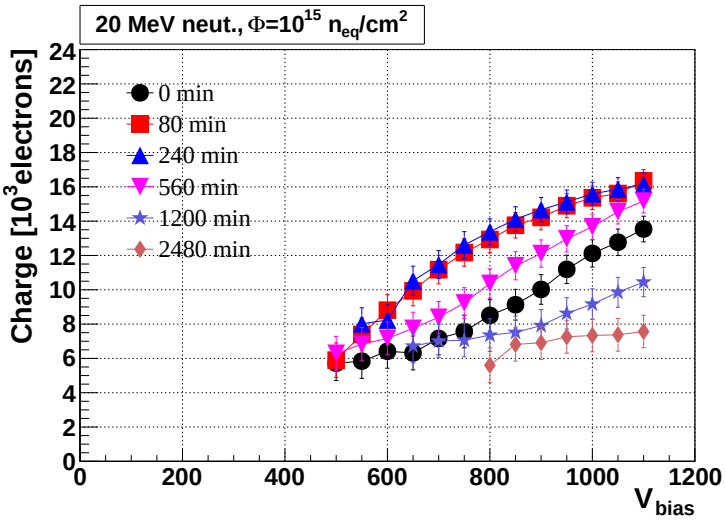

Figure 8. Cluster charge vs. V_{bias} at different annealing steps for the sensor irradiated with neutrons at $1{\cdot}10^{15}\,n_{eq}/cm^2$.

with a corresponding higher charge at 500 V. However, the same charge as in the corresponding neutron irradiated sample is collected for the highest voltage applied in this work.

The last CCE annealing plot (figure 11) refers to the case of the sensor irradiated with an equal fluence of protons and neutrons. The cluster charge at 500V (see figure 14) and the depletion voltage (see figure 15) are compatible with the results obtained with the same equivalent fluences of protons or neutrons only. The cluster charge and the depletion voltage assume intermediate values with respect to the values obtained for the sensors irradiated with neutrons or protons only. For the measurements taken after 240 minutes at 60°C, a significant drop in the cluster charge was observed (see figure 14). The behaviour, which proved to be reproducible, is not visible at longer annealing times and remains unexplained.

2015 JINST 10 P08005

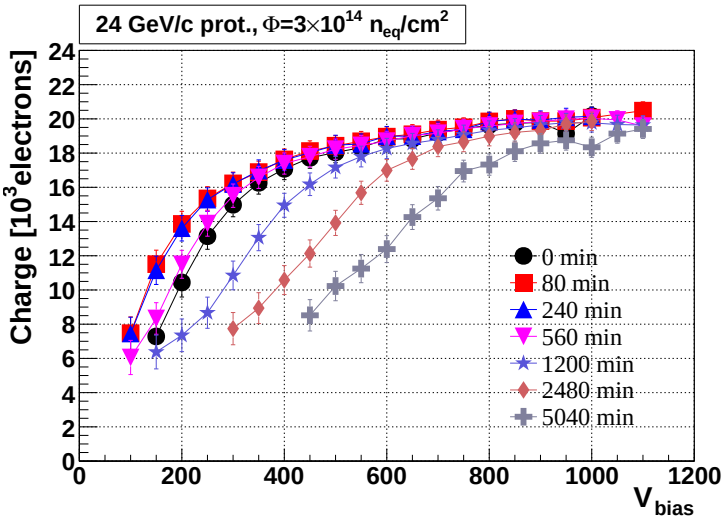

Figure 9. Cluster charge vs. V_{bias} at different annealing steps for the sensor irradiated with protons to $3{\cdot}10^{14}\,n_{eq}/cm^2$.

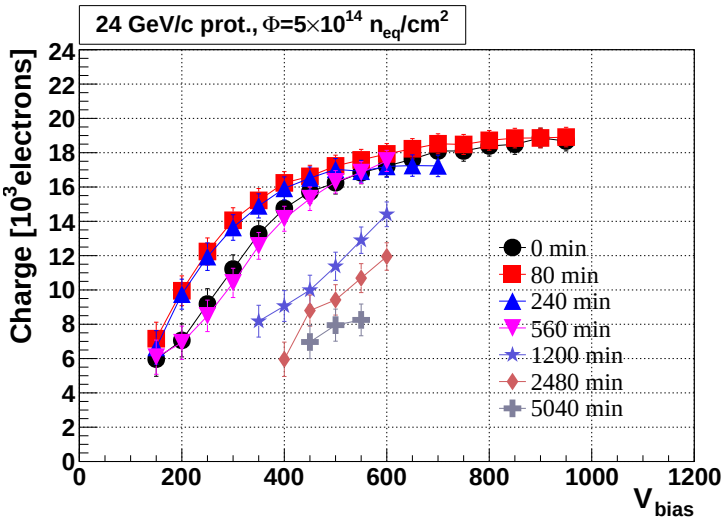

Figure 10. Cluster charge vs. V_{bias} at different annealing steps for the sensor irradiated with protons at $5{\cdot}10^{14}\,n_{eq}/cm^2$.

In the present LHC experiments the maximum voltage of the power supplies for most of the strip trackers are limited to 500 V. For this reason, cluster charge values at this bias voltage are plotted as a function of annealing time in figure 12. Cluster charge values are only heavily affected by annealing for sensors irradiated to at least $3 \cdot 10^{14} n_{eq}/cm^2$. A bigger effect of beneficial annealing is observed in neutron irradiated sensors, though one should be reminded that proton irradiation was performed at room temperature. Thus it can be argued that most of the beneficial annealing took place while the sensor was still in the beam (a few days at $\sim$27°C). At longer annealing times a decrease in the cluster charge for all samples irradiated with $3 \cdot 10^{14} n_{eq}/cm^2$ and above can be observed, with proton irradiated sensors showing a systematically higher value of cluster charge than neutron irradiated ones (see for example figure 12).

2015 JINST 10 P08005

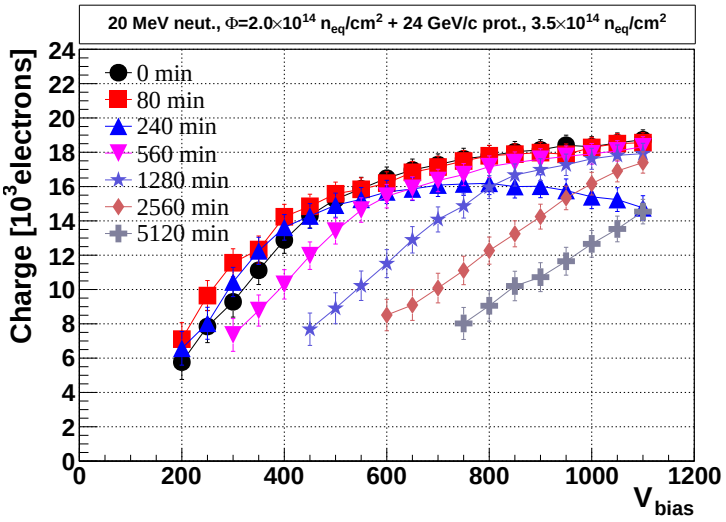

Figure 11. Cluster charge vs. V_{bias} at different annealing steps for the mixed irradiated sensor.

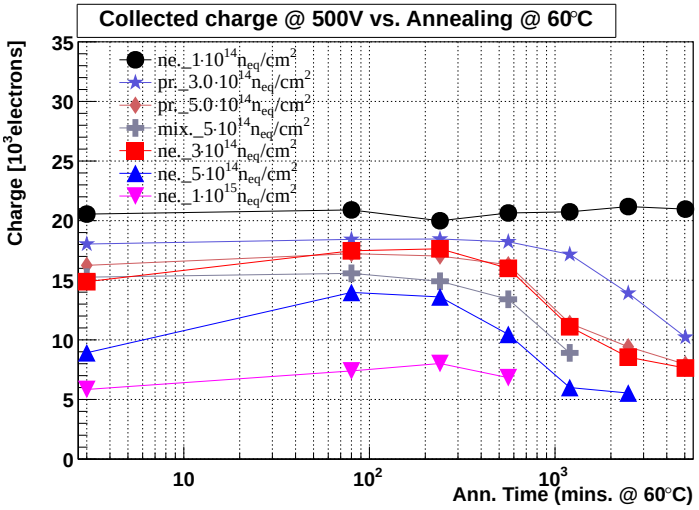

Figure 12. Values of cluster charge at 500 V as a function of annealing time for the different fluences.

Figure 13 shows the cluster charge vs. voltage at an annealing time of 2480 minutes at 60°*C* for the different investigated fluences. The plot demonstrates well how the depletion voltage increases and the charge collections decreases at V_{dep} for all sensors irradiated to more than $1 \cdot 10^{14}\,n_{eq}/cm^2$. The comparison also shows the lower depletion voltage observed in proton irradiated samples with respect to neutron irradiation for equivalent fluences which is systematically observed for all annealing times (see figure 15).

At each annealing step, a pedestal run with internal triggering of the readout electronics was also performed, in order to extract average strip *Equivalent Noise Charge* (ENC) values at each annealing step. The values are shown in figure 14.

Noise charge results to be quite constant with annealing, regardless of the depletion status of the sensor. Moreover no clear correlation can be noticed between noise charge and irradiation

2015 JINST 10 P08005

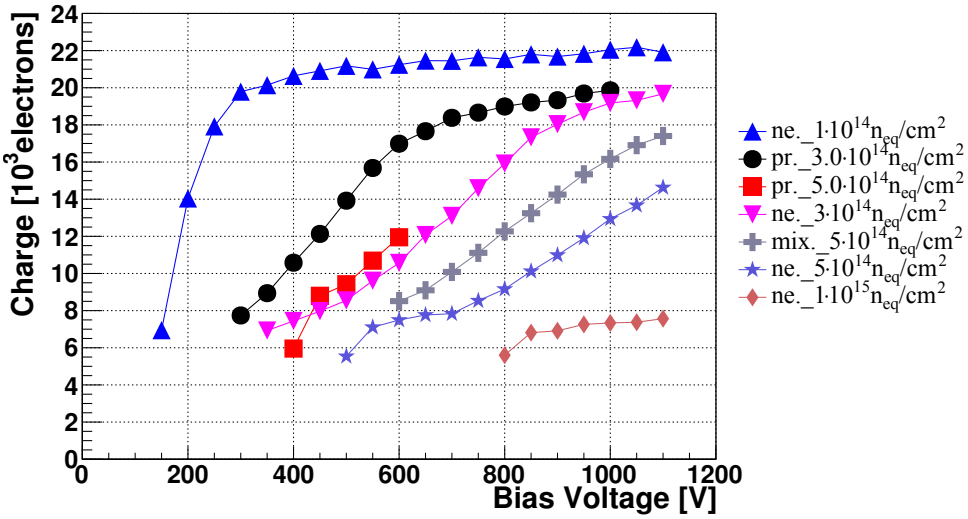

Figure 13. Comparison of cluster charge vs. bias voltage at 2480 minutes of annealing at 60°C.

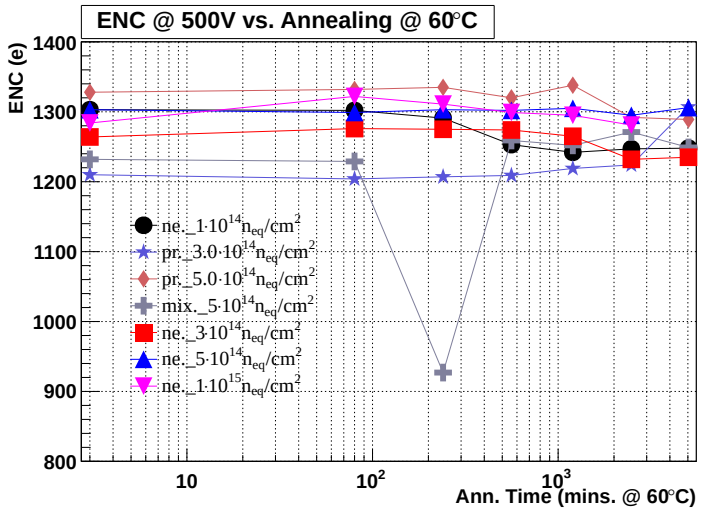

Figure 14. Values of strip *Equivalent Noise Charge* at 500 V as a function of annealing time for the different fluences.

fluence, indicating that the noise was dominated by the capacitive component in the measurements. One point corresponding to 240 minutes of annealing for the mixed irradiated detector shows an anomalously low noise charge. This is the same annealing stage at which, for the mixed irradiated detector, a decreasing behavior of cluster charge with voltage was observed (figure 11). Since the two measurements (cluster charge and noise) were taken separately, a systematic error related to the CCE set-up can be excluded, and the anomalous behavior should be attributed to the sensor itself, though no explanation is proposed for it. Finally, V_{dep} values were extracted for each sensor, at each annealing step, from the cluster charge (Q_{clust}) vs. voltage characteristics. The extraction was performed by plotting the $1/Q^2_{clust}$ vs. V_{bias} and then fitting two straight lines to the rising slope and the region of saturated charge. Figure 15 shows the extracted values of depletion voltage

2015 JINST 10 P08005

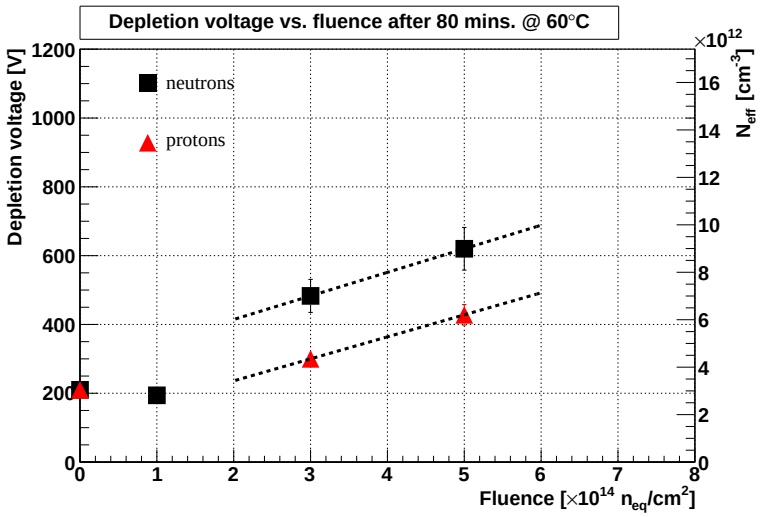

Figure 15. Depletion voltages as a function of fluence at the annealing minimum. The dotted lines represents the fits performed for fluences $\geq 3 \cdot 10^{14}\,\mathrm{n_{eq}/cm^2}$, well above type inversion expected for this type of sensor. For explanation about the derivation of N_{eff} refer to [10].

as a function of irradiation fluence at the annealing minimum. In this condition it is possible to extract an estimate for the g_c (stable damage introduction rate) value by a linear fit on the points at higher fluences, where the type inversion has completely occurred. Such fit provided the values $(0.99 \pm 0.56)\,10^{-2}\mathrm{cm}^{-1}$ and $(0.92 \pm 0.38)\,10^{-2}\mathrm{cm}^{-1}$ for neutrons and protons, respectively. The large errors derive from the fact that since only two points were available for each fit, errors were only propagated from the accuracy by which the depletion voltage was extracted through manual fitting (as described above), assumed to be in the order of 10%. The obtained values for g_c are compatible with values obtained by the Capacitance-Voltage characterization in previous works performed on the same type of sensors, where a $g_c = (1.22 \pm 0.05)\,10^{-2}\mathrm{cm}^{-1}$ was found [25]. Figure 16 shows the depletion voltage as a function of annealing time for all sensors. The data were fitted using the empirical parametrization for N_{eff} proposed by the Hamburg model [10]:

$$\begin{aligned}\Delta N_{\mathrm{eff}}(\Phi_{\mathrm{eq}}, t(T_a)) \;=\; & N_{C0}(1-\exp(-c\Phi_{\mathrm{eq}})) + g_c\Phi_{\mathrm{eq}} \\ & + g_a\Phi_{\mathrm{eq}}\exp(-t/\tau_a) + N_{Y,\infty}\left(1 - \frac{1}{1+t/\tau_Y}\right)\end{aligned} \tag{4.1}$$

with $\Delta N_{\mathrm{eff}} = N_{\mathrm{eff},0} - N_{\mathrm{eff}}\left(\Phi_{\mathrm{eq}}, t(T_a)\right)$ being the difference of the effective doping concentration measured before and after irradiation. In the fit only two parameters were left free, namely the donor-removal component ($N_{C0}(1-\exp(-c\Phi_{\mathrm{eq}}))$, considered as a single parameter) and the long term damage parameter ($N_{Y,\infty}$). The former term is strongly material dependent and no reliable parametrization was found in literature for the material used. All remaining parameters were taken from [10], with the exception of the g_c term, which was extracted from the curves plotted in figure 15. Values for $N_{Y,\infty}$ are listed in table 2.

The linear fit on the $N_{Y,\infty}$ as a function of irradiation fluence returns an introduction rate of $(3.74 \pm 0.02)\,10^{-2}\mathrm{cm}^{-1}$, about 20% lower than the average value from [10]. It should be noted, however, that this quantity shows a variance between different silicon materials, most probably

2015 JINST 10 P08005

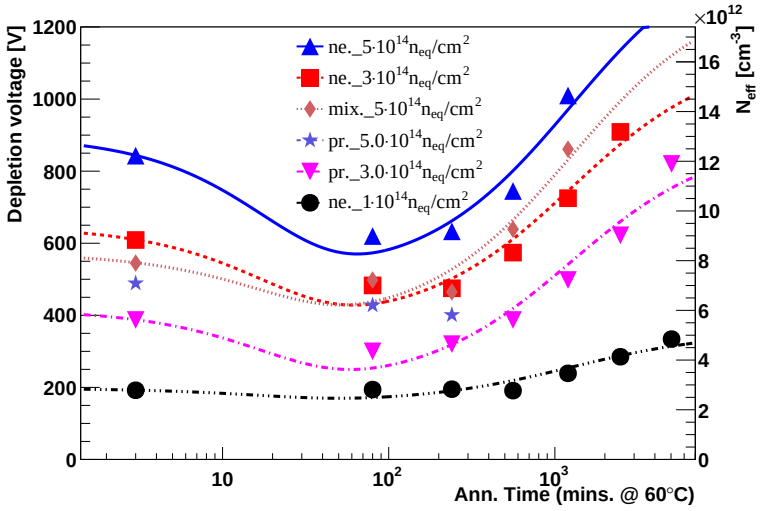

Figure 16. Depletion voltages vs. annealing time, extracted from the cluster charge vs. voltage characteristic.

Table 2. $N_{Y,\infty}$ values extracted from the fits on the curves plotted in figure 16.

Fluence (n_{eq}/cm^2)	Particles	$N_{Y,\infty}[cm^{-3}]$
$1.0 \cdot 10^{14}$	neut.	$0.34 \pm 0.04 \cdot 10^{13}$
$3.0 \cdot 10^{14}$	neut.	$1.19 \pm 0.10 \cdot 10^{13}$
$5.0 \cdot 10^{14}$	neut.	$1.74 \pm 0.29 \cdot 10^{13}$
$3.0 \cdot 10^{14}$	prot.	$1.12 \pm 0.01 \cdot 10^{13}$
$5.0 \cdot 10^{14}$	mix.	$2.04 \pm 0.48 \cdot 10^{13}$

depending on oxygen concentrations. Agreement with the Hamburg model is poor, on the other hand, for the extracted beneficial annealing parameter, which relies on a single data point only. Finally, one should consider that V_{dep} was extracted from cluster charge vs. bias voltage curves which are strongly affected by trapping in this work and thus might be different from the values obtained from CV characteristics.

5 Edge-TCT measurement

Annealing was stopped at 2480 minutes for the sensor irradiated to the highest neutron fluence ($1 \cdot 10^{15}\, n_{eq}/cm^2$). At this stage, it was in fact not possible anymore to fit a Landau function with a convoluted Gaussian function to the cluster charge distribution for voltages lower than 800 V. It was hence decided to perform an Edge-TCT measurement on the sensor, using the set-up described in [24] in order to investigate the extremely low value of cluster charge observed in CCE measurements using electrons from a ^{90}Sr source. This technique uses of a pulsed infrared laser (80 ps pulse width) to generate a localized charge cloud in the bulk. The laser light is projected in the detector plane, perpedicularly to the strip direction. The laser is focused under a single strip whose signal

2015 JINST 10 P08005

is then read through an oscilloscope after having been amplified. By analyzing the resulting transient signals induced on the strip for different injection depths, one can extract information about the local electric field. A detailed description of the data analysis methods can be found in [26]. The corresponding plots for drift velocity and charge collection efficiency (the latter with a 25 ns integration window over the transient pulse) are shown in figures 17 and 18 respectively.

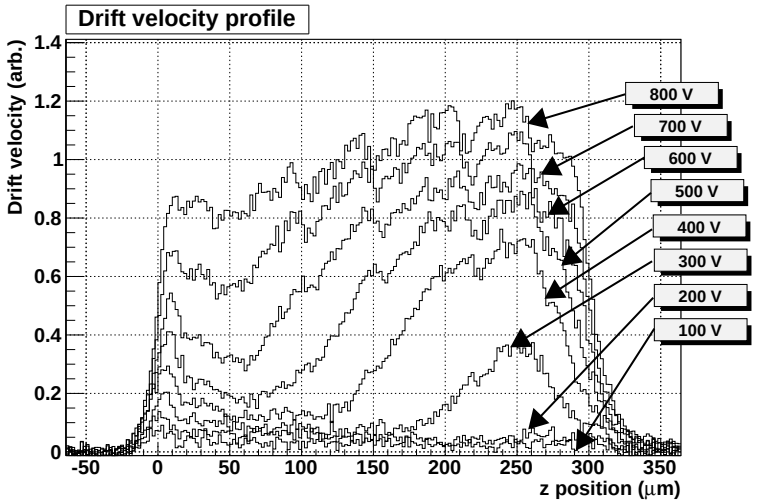

Figure 17. Drift velocity as function of generation depth for sensor irradiated at 10^{15}n/cm^2 after 2480 minutes of annealing at 60°C.

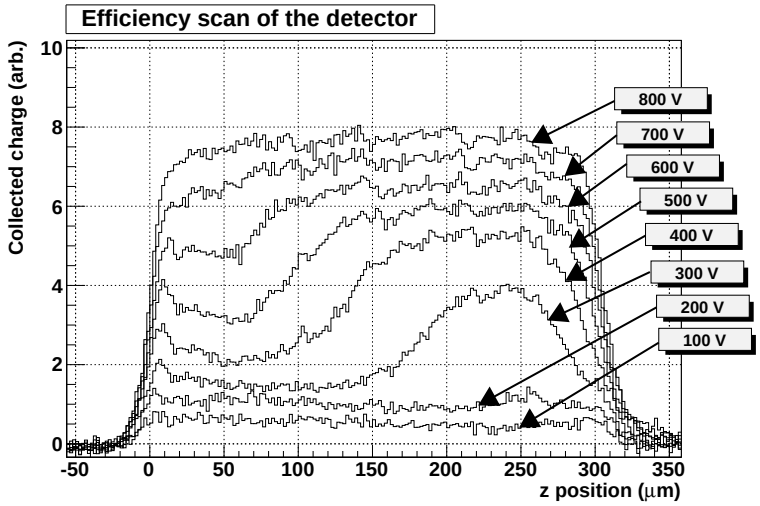

Figure 18. Efficiency of charge collection as function of generation depth for sensor irradiated at 10^{15}n/cm^2 after 2480 minutes of annealing at 60°C.

Figure 17 shows a drift velocity (and hence field) profile developing from the ohmic contact of the sensor (z=300 μm). A narrow region with high field can be noticed on the strip side (z=0). Figure 18 shows the efficiency profile of the sensor.

2015 JINST 10 P08005

It should be noted that in the measurement conditions for Edge-TCT, the weighting field is the one of a PAD detector even though a strip detector is used for the measurement. The reason is found in the fact that the charge is generated homogeneously in a light tunnel crossing underneath several strips. A detailed explanation is given in [26].

This is different from the situation where a source is used, since the charge is generated in a localized volume concerning one or two strips only. Here the weighting field of a strip detector is to be applied to understand the signal generation.

The low values for cluster charge observed with beta source measurements can thus be correlated to the poor overlapping of the high electric field and high weighting field regions of one strip [7]. The weighting field for this sensor geometry is significant only for the first 50 μm under the strip [27].

Figure 18 shows how the electric field in the strip region is low and has a limited depth extension. Charge carriers generated close to the ohmic contact are likely to be trapped before reaching the high weighting field region. The low electric field in the region between 50 and 100 μm, corresponding to a low drift velocity, increases the collection time for charge carriers, thus increasing their probability of being trapped.

6 Discussion of results

In the present work we have extensively characterized FZ p-on-n silicon strip sensors using a set-up for charge collection measurements with β particles to understand the charge collection properties of these sensors with annealing after irradiation. Although long annealing times have been investigated (the last step corresponding to $\sim$ 5 years at room temperature), they could be easily reached if sensors are not properly cooled throughout their operation: for example an increase of the sensor temperature to 40°C would imply a factor 17 (29 for the long term annealing) in the annealing rate with respect to 20°C [10]. Sensor performance does not seem to be affected up to fluences of $1 \cdot 10^{14}\,\mathrm{n_{eq}/cm^2}$, as long as a bias of 500 V can be provided. However higher fluences will require major care in keeping the sensors cold, as the cluster charge at 500 V could drop to values as low as $\sim$6,000 e^- after irradiation with $3 \cdot 10^{14}\,\mathrm{n_{eq}/cm^2}$. A similar, recent work [28] has been published, determining the cluster charge annealing behavior of p-on-n sensors irradiated with reactor neutrons to a fluence of $2 \cdot 10^{14}\,\mathrm{n_{eq}/cm^2}$. The reported cluster charge falls in between the values observed in this work for the sensors irradiated with neutrons to fluences of $1 \cdot 10^{14}\,\mathrm{n_{eq}/cm^2}$ and $3 \cdot 10^{14}\,\mathrm{n_{eq}/cm^2}$.

Further studies of the silicon material properties were performed to assess doping profiles and oxygen concentration in the studied sensors. These measurements were performed to provide a reference when comparing the results presented in this work with other similar measurements in literature on sensors produced by different manufactures. An Edge-TCT measurement was finally performed on a sensor where, due to high radiation fluence and annealing, almost no signal was visible anymore. This measurement led to the conclusion that the main reason for signal loss is related to the development of the depleted volume starting from the backside ohmic contact, where the weighting field of the readout electrodes is lower.

2015 JINST 10 P08005

Acknowledgments

We would like to thank Maurice Glaser for the support at the 24 GeV/c irradiation facility at CERN and the colleagues at Louvain-la-Neuve irradiation facility for the neutron irradiations. The work was performed in the framework of the RD50 collaboration and in part supported by the Marie Curie FP7 Training Network MC-PAD.

References

[1] ATLAS collaboration, *Atlas Pixel Detector Technical Design Report*, ATLAS-TDR-11, CERN/LHCC 98-13 (1998).

[2] CMS collaboration, *Tracker Technical Design Report* (2000).

[3] ATLAS collaboration, *ATLAS inner detector: Technical design report. Vol. 1*, CERN-LHCC-97-16, ATLAS-TDR-4 (1997).

[4] G. Kramberger, *Signal development in irradiated silicon detectors*, Ph.D. Thesis, Ljubljana University, Ljubljana Slovenia (2001).

[5] W. Shockley, *Currents to Conductors Induced by a Moving Point Charge*, *J. Appl. Phys.* **9** (1938) 635.

[6] S. Ramo, *Currents Induced by Electron Motion*, *Proc. IRE* **27** (1939) 583.

[7] K. Iniewski, *Radiation Effects in Semiconductors*, CRC Press, Boca Raton U.S.A. (2011).

[8] (INFN, Bari), *Technical Proposal for the Phase-II Upgrade of the CMS Detector*, CERN-LHCC-2015-010 (2015).

[9] ATLAS collaboration, *Letter of Intent for the Phase-II Upgrade of the ATLAS Experiment*, CERN-LHCC-2012-022 (2012).

[10] M. Moll, *Radiation Damage in Silicon Particle Detectors - microscopic defects and macroscopic properties*, Ph.D. Thesis, University of Hamburg, Hamburg Germany (1999).

[11] B. Dezillie, F. Lemeilleur, M. Glaser, G.L. Casse and C. Leroy, *Experimental results on radiation induced bulk damage effects in float zone and epitaxial silicon detectors*, *Nucl. Instrum. Meth.* **A 386** (1997) 162.

[12] A. Ruzin, G. Casse, M. Glaser, A. Zanet, F. Lemeilleur and S. Watts, *Comparison of radiation damage in silicon induced by proton and neutron irradiation*, *IEEE Trans. Nucl. Sci.* **46** (1999) 1310.

[13] L. Beattie, T.J. Brodbeck, A. Chilingarov, G. Hughes, P. Ratoff and T. Sloan, *Charge collection efficiency in heavily irradiated silicon diodes*, *Nucl. Instrum. Meth.* **A 412** (1998) 238.

[14] M.M. Angarano et al., *Study of radiation damage and substrate resistivity effects from beam test of silicon microstrip detectors using LHC readout electronics*, *Nucl. Instrum. Meth.* **A 488** (2002) 85.

[15] P.P. Allport et al., *Charge collection efficiency studies with irradiated silicon detectors*, *Nucl. Instrum. Meth.* **A 501** (2003) 146.

[16] Hamamatsu website, http://www.hamamatsu.com.

[17] A. Barcz, M. Zielinski, E. Nossarzewska and G. Lindström, *Extremly deep SIMS profiling: oxygen in FZ silicon*, *Appl. Surf. Sci.* **203-204** (2003) 396.

[18] CERN-RD-48 collaboration, A. Ruzin, *Recent results from the RD-48 (ROSE) collaboration*, *Nucl. Instrum. Meth.* **A 447** (2000) 116.

2015 JINST 10 P08005

[19] ROSE collaboration, G. Lindström et al., *Developments for radiation hard silicon detectors by defect engineering — Results by the CERN RD48 (ROSE) collaboration*, *Nucl. Instrum. Meth.* **A 465** (2000) 60.

[20] I. Pintilie, G. Lindstroem, A. Junkes, E. Fretwurst, *Radiation-induced point- and cluster-related defects with strong impact on damage properties of silicon detectors*, *Nucl. Instrum. Meth.* **A 611** (2009) 52.

[21] CERN-ROSE/RD48 collaboration, M. Glaser, L. Durieu, F. Lemeilleur, M. Tavlet, C. Leroy and P. Roy, *New irradiation zones at the CERN PS*, *Nucl. Instrum. Meth.* **A 426** (1999) 72.

[22] K. Bernier et al., *An intense fast neutron beam in Louvain-la-Neuve*, http://www.fynu.ucl.ac.be/.

[23] ALIBAVA collaboration, R. Marco-Hernandez, *A portable readout system for silicon microstrip sensors*, *Nucl. Instrum. Meth.* **A 623** (2010) 207.

[24] N. Pacifico, I. Dolenc Kittelmann, M. Fahrer, M. Moll and O. Militaru, *Characterization of proton and neutron irradiated low resistivity p-on-n magnetic Czochralski ministrip sensors and diodes*, *Nucl. Instrum. Meth.* **A 658** (2011) 55.

[25] A.J. Furgeri, W. de Boer, F. Hartmann, S. Freudenstein, S. Assouak and E. Forton, *Radiation damage effects on CMS sensors quality assurance and irradiation tests*, *IEEE Trans. Nucl. Sci.* **51** (2004) 3063.

[26] G. Kramberger et al., *Investigation of Irradiated Silicon Detectors by Edge-TCT*, *IEEE Trans. Nucl. Sci.* **57** (2010) 2294.

[27] H. Spieler, *Semiconductor Detector Systems*, *Oxford Science Publications*, Oxford University Press, Oxford U.K. (2005).

[28] P.J. Dervan, C. Wiglesworth, J. Vossebeld, G. Casse, A. Affolder and A. Greenall, *Update of the annealing scenario for irradiated silicon p-in-n microstrip sensors*, *Nucl. Instrum. Meth.* **A 658** (2011) 17.

2015 JINST 10 P08005